Time-dependent dynamics of an intense laser-induced above-threshold Coulomb explosion

B. D. Esry and I. Ben-Itzhak

J.R. Macdonald Laboratory and Department of Physics, Kansas State University, Manhattan, Kansas 66506, USA

(Received 26 July 2010; published 8 October 2010)

We use our recently proposed model to extract information about the nuclear dynamics from the Coulomb explosion data of Staudte *et al.* [Phys. Rev. Lett. **98**, 073003 (2007)]. Those data, taken at multiple intensities near the ionization appearance intensity for both H_2 and D_2 in linearly and circularly polarized light, show remarkable structure and regularity not easily explained by conventional models. Because our model does fit the spectra well, we can infer the qualitative time-dependent evolution of the system. In addition, it suggests a possible experimental signature of rescattering leading to above-threshold Coulomb explosion.

DOI: 10.1103/PhysRevA.82.043409 PACS number(s): 33.80.Rv, 33.80.Wz, 42.50.Hz

I. INTRODUCTION

It is well known that experimental measurements of the relative kinetic energy of the protons following double ionization of H_2 or single ionization of H_2^+ by an intense laser pulse yield a broad relatively featureless distribution [1,2]. The accepted explanation of this Coulomb explosion process is called charge resonance-enhanced ionization (CREI) [3], although definitive experimental evidence of the often-predicted multiply peaked CREI distribution has proven elusive [4,5]. This mechanism is understood from a static electric field static nuclei picture much like strong-field tunneling ionization in atoms [6].

Recent experiments, however, have revealed richer than expected structure in the kinetic-energy release (KER) spectrum for laser intensities near the ionization appearance intensity [7,8]. In this intensity regime, the Keldysh parameter—which characterizes the extent to which ionization in an intense laser can be considered tunneling or multiphoton [6]—is near unity for all important internuclear distances R, so both pictures can be expected to provide insight.

We have proposed a model to explain this KER structure [8], and in this paper, we apply that model to the experimental data of Staudte *et al.* [7]. In the process, we will gain a deeper understanding of the intriguing ionization dynamics behind the structure. This is possible, in part, because our model [8] unifies the description of dissociation and ionization, allowing them to be discussed using the same concepts and language. Furthermore, it ties the initiating dissociation mechanism in a natural way to the ionization process and resulting KER, revealing the time dependence of H_2^+ Coulomb explosion. Our model explains nearly all of the features of the Staudte *et al.* data, and we propose other experiments to both test our model and uncover interesting physics.

Since Staudte *et al.* used both linearly and circularly polarized light as well as two different isotopes, their data provide a comprehensive test of our model. In addition, beginning from a neutral H_2 target leads to nontrivial differences from the H_2^+ beam results in Ref. [8]. First, the resulting H_2^+ ions do not experience the full laser pulse, only that part of the pulse following the first ionization. Second, the initial H_2^+ vibrational distributions are different. The H_2^+ molecules in the beam are in an *incoherent* Franck-Condon distribution of vibrational states. The H_2^+ molecules produced in the laser pulse are in a *coherent* superposition of vibrational states that is most likely shifted toward lower states than Franck-Condon [9]. Third, for H_2 in linearly polarized light, it is possible for the first ionized electron to recollide with the H_2^+ remnant, leading to physical processes clearly not possible for the H_2^+ beam.

II. MODEL

Our model has its roots in the Floquet potentials that have long been used to describe laser-induced dissociation of H_2^+ into $p + H$ [6,10]. The *diabatic* Floquet potentials are produced by adding an index n to the field-free Born-Oppenheimer potentials that represents the number of photons exchanged with the laser field. For instance, if $n = -1$, one photon has been absorbed from the field, and the corresponding Born-Oppenheimer potential is shifted down in energy by $\hbar\omega$ where ω is the laser carrier frequency. The potentials are then coupled according to the electric dipole selection rules. The *adiabatic* Floquet potentials are generated by diagonalizing the diabatic potential matrix. The adiabatic potentials have led to the identification of the main physical mechanisms of dissociation: bond softening (BS), vibrational trapping (VT), and above-threshold dissociation (ATD) [6,10]. These different pathways are indicated schematically in Fig. 1 along with the adiabatic Floquet potentials for dissociation.

The key step of our model is to add potential curves representing ionization to the Floquet picture. Figure 1 shows these potentials diabatically [i.e., $1/R - n\omega$ in atomic units (which will be used hereafter unless otherwise noted)]. More precisely, these are the ionization threshold potentials, as they assume the photoelectron was "born" with zero energy. Where one of these curves crosses a dissociation curve, that channel opens, and ionization can occur. By their nature, these channel openings are quasistationary with respect to intensity and will thus be emphasized in the intensity average inherent in experiments. A wave packet that dissociates via BS crosses three ionization threshold potentials in the range of the figure. Transitions at each of these crossings yield a peak in the ionization KER spectrum. Their energies are the sum of the kinetic energy accumulated during dissociation and that gained on the ionization potential, or, more simply, the difference between the initial energy and the asymptotic ionization potential thresholds $-n\omega$. Since these thresholds are separated by ω, the ionization KER spectrum shows a sequence of peaks separated by the photon energy—a phenomenon we have labeled above-threshold Coulomb explosion (ATCE) [8].

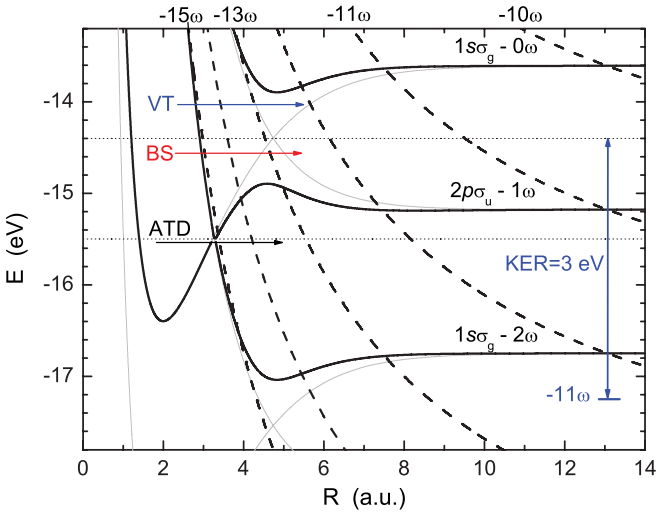

FIG. 1. (Color online) The Floquet potentials for H_2^+ at 800 nm: adiabatic dissociation potentials at 10^{13} W/cm^2 (solid black lines), diabatic dissociation potentials (thin solid gray lines), and diabatic ionization potentials (dashed black lines). The curves are labeled by the associated number of photons absorbed from the field, with the $R \to \infty$ limit of the -11ω ionization curve indicated as an example. The various dissociation mechanisms that initiate the above-threshold Coulomb explosion (ATCE) ionization—VT, BS, and ATD—are sketched at roughly the energy where they are most important.

In most cases, this sequence will overlap the ATCE peaks initiated by ATD as well as any peaks initiated by VT.

At first glance, combining adiabatic and diabatic potential curves may seem strange. This choice, however, is appropriate for H_2^+ produced in an already intense laser. The few-photon coupling between the dissociative curves is much stronger than the ten-photon (or more) coupling to the ionization curves—the coupling at a crossing between n- and m-photon curves is roughly proportional to $(\mathcal{E}D)^{|n-m|}$, where $\mathcal{E}$ is the laser electric field and D is the dipole matrix element. So, when H_2 is ionized to produce H_2^+, there is a large preexisting intensity-dependent coupling between the $1s\sigma_g - 0\omega$ and $2p\sigma_u - 1\omega$ curves. The adiabatic dissociation Floquet curves display this physics visually in the form of an avoided crossing. Besides this physical motivation, our goal is to keep this model as simple as possible—and, while the adiabatic curves for dissociation are relatively easy to obtain, the adiabatic curves including ionization are not.

The time dependence of the laser pulse envelope $\mathcal{E}(t)$ can be included in these potential curves rigorously [11], but we need only the qualitative effect here. The Floquet curves already account for the fast oscillation of the carrier, and the slow variation of $\mathcal{E}(t)$ can be included in the coupling. For the adiabatic curves, this time dependence is reflected in the size of the gap at the avoided crossings. The one-photon BS gap, for instance, is proportional to $\mathcal{E}(t)D$ to lowest order in $\mathcal{E}(t)D$. For the diabatic curves, the time dependence is entirely in the coupling elements via $\mathcal{E}(t)$.

III. RESULTS AND DISCUSSION

Whether a particular peak appears in the KER spectrum depends on the vibrational wave packet reaching the associated crossing or avoided crossing during the laser pulse, giving us a window into the time-dependent nuclear dynamics. Upon ionization of H_2, for example, a portion of the H_2^+ vibrational wave packet has energies lying in the ATD gap that reach the gap a little less than 10 fs after the first ionization. (This time can be estimated using the fact that the nuclei in H_2^+ take about 2.7 fs to move 1 a.u. with 1 eV of kinetic energy; the equivalent time for D_2^+ is $\sqrt{2}$ longer, or about 3.8 fs.) This dissociating wave packet encounters the 15ω ionization curve in the ATD gap, and can travel through three more crossings to reach the 12ω crossing within the 40 fs of the laser pulse. It follows that the presence or absence of a peak in the KER spectrum is a strong indication of the dynamical mechanism leading to that peak. For instance, for the same peak intensity, a long pulse will lead to lower KER peaks than a short pulse.

The positions and widths of the KER peaks can also reveal dynamical information, since the initial dissociating wave packet is intensity—and thus time—dependent. For instance, if we can identify the BS-to-13ω peak in the ionization KER spectrum, its position indicates the laser intensity when the wave packet reached the BS barrier. This conclusion follows from the fact that the mean energy of the BS wave packet lies just above the top of the BS barrier, since the vibrational distribution of the initial wave packet is maximal at energies below the $2p\sigma_u - 1\omega$ threshold and decreases across the BS energy range. The laser pulse is already near its peak when H_2 is ionized and this wave packet is formed, so the BS barrier is nearly gone—the barrier for 10^{13} W/cm^2 in Fig. 1 is quite low, and ionization of H_2 requires even larger intensities. Similar logic applies for the peak widths so that large-R crossings tend to produce narrower (and lower) KER peaks. We know that anything ionized at large R necessarily dissociated early in the pulse over a narrow range of intensities precisely because it arrived at large R while there was still sufficient intensity to ionize. Conversely, crossings at small R tend to give broad, high-KER peaks since they are fed from a broad range of intensities during the pulse. Further, since the couplings are proportional to the electric field, all of the peaks tend to broaden with increasing intensity. These predictions of our model were seen in our data [8] for H_2^+ and are also clearly seen in the H_2 data of Staudte *et al.* [7] shown in Fig. 2.

A. Staudte *et al.* data

Besides the structure itself, Fig. 2 shows other curious features: The peaks for H_2^+ are in essentially the same place for all intensities and for both linearly and circularly polarized light. Moreover, the peaks for D_2^+ show only a small shift of all peaks to higher KER relative to H_2^+. Can we explain these observations with our model?

Per the arguments above, we do expect the low-KER (large-R) peak positions to be approximately independent of intensity, but anticipate that the large-KER (small-R) peaks would shift. We attribute the lack of a clear shift of these latter peaks to the fact that the H_2^+ is created with the BS and ATD barriers already suppressed, which stay suppressed while the bulk of the wave packet dissociates. Also, the intensity average over the laser focal volume accentuates low intensities.

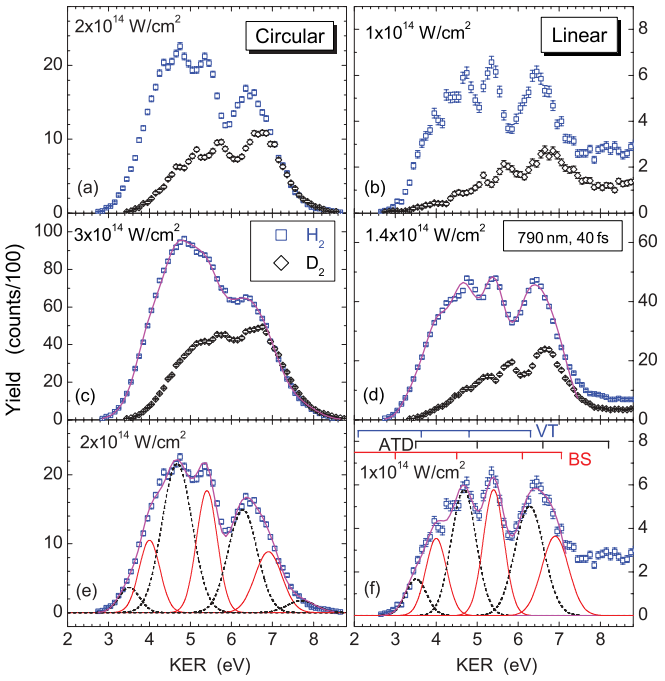

FIG. 2. (Color online) H_2 and D_2 Coulomb explosion KER spectra from Staudte *et al.* [7] for circular (left column) and linear (right column) polarizations. The laser pulse length was 40 fs with a central wavelength of 790 nm. Panels (e) and (f) show our model fit to the H_2 data in (a) and (b), respectively, both individual peaks and total. The bars in (f) indicate the diabatic peak positions grouped by mechanism. In (e) and (f), the solid red lines indicate the individual BS-initiated peaks; and the dashed black lines, ATD-initiated peaks. The thick solid purple lines in (c)–(f) are the total fitted spectra.

The peak positions for circularly polarized light can be explained using our model and Fig. 1 by recognizing that for the parallel transitions most important here, only the projection of the electric field on the molecular axis matters. Assuming that nuclear rotation can be ignored in these short pulses, this projection just gives linearly polarized light in the molecular frame, so the potentials in Fig. 1 still apply as do all of our earlier discussions. Since care was taken in the experiment to ensure that the maximum field was the same for both polarizations, it is thus not surprising that the spectra look similar.

There are, however, clear differences between the polarizations. For energies above roughly 7.5 eV, the differences are due primarily to rescattering effects beyond the present model. Below 7.5 eV, our model does apply, and the differences can be ascribed to geometrical alignment. If we imagine the sphere representing the electric-field vector, with linearly polarized light along the poles and circularly polarized light at the equator, then the equatorial plane is depleted in circularly polarized light, while only the polar axis is depleted in linearly polarized light. This simple geometrical picture shows that the ratio of the sphere's surface in high intensities to that in low intensities is higher for circularly polarized light than for linearly polarized light. We know, though, that higher intensities tend to broaden the peaks and will contain a higher proportion of large-R low-KER peaks, since the pulse retains enough intensity at the long times needed to reach the large-R crossings. Both effects can be seen by comparing Figs. 2(a) to 2(b) and Figs. 2(c) to 2(d).

B. Fitting the data

Our model's predictions can be tested more quantitatively by using it to fit the data in Fig. 2. If our model is correct, we should be able to use essentially the same parameters for the positions and widths of all the spectra in Fig. 2 with some small adjustments for intensity. Simultaneously fitting several spectra provides constraints beyond those from our model and is an iterative process that reveals further physics. For instance, should there be any structure in the linearly polarized spectra not reproduced by the simultaneous fit with circular polarization, rescattering is the most likely candidate.

Figure 1 has several crossings that might lead to peaks whose positions, based on completely diabatic curves, are indicated by the bars in Fig. 2(f). Although present for H_2^+ [8], we do not expect VT-initiated peaks for H_2 due to the small probability of a nonadiabatic transition at the BS barrier to the VT well. Further, the population of vibrational states at the needed energies is even smaller than for H_2^+. So, limiting ourselves to only BS- and ATD-initiated ionization, we have ten possible peaks. Comparing with the data, we can immediately eliminate the 10ω and 11ω peaks from BS and the 11ω peak from ATD as none give a KER higher than 3.0 eV. The remaining seven peaks cannot be eliminated, but we do expect that the 8.2-eV 15ω ATD peak and the 7.1-eV 14ω BS peak will be small, since they require the highest number of photons; but, if present, they should show up more prominently in the circularly polarized data given their higher average intensities. As the 8.2-eV peak lies at a KER with known rescattering contributions, we exclude it from our simultaneous fit of the two polarizations. It is, however, individually fit to the circular polarization data after the parameters for the remaining peaks have been determined through the simultaneous fit.

Figures 2(e) and 2(f) show the results of our fit to the H_2 data. Each Gaussian has, in principle, three parameters, giving a total of 36 between the two polarizations. Our model predicts the peak positions and imposes some constraints on their widths, allowing the total number of free parameters to be roughly halved [8]. As further validation of our model, we took the parameters determined from the fit to the lower-intensity data and, allowing only an overall scaling of the peaks' width and height, fit the higher-intensity data as well. The resulting spectra are shown in Figs. 2(c) and 2(d).

The three ATD-initiated peaks show a small $\sim$0.2-eV shift downward from their diabatic position, consistent with the shift of the ATD barrier at $\sim 5 \times 10^{13}$ W/cm^2 as determined from the adiabatic Floquet potentials. This intensity is reasonable for the first ionization of H_2. Moreover, this sequence of peaks, spaced by ω, is an example of ATCE [8]. As expected, the two BS-initiated peaks are strongly shifted from the diabatic prediction indicated by the bars. From the fit, the 13ω BS peak lies at 5.35 eV—a 0.75-eV shift from the diabatic result—which translates into a mean-kinetic energy of about 0.1 eV for the dissociating BS wave packet. As discussed before, this shift reveals the intensity at which the wave packet passed over the BS barrier. In this case, because the shift is consistent with the nearly complete suppression of the barrier, we can only

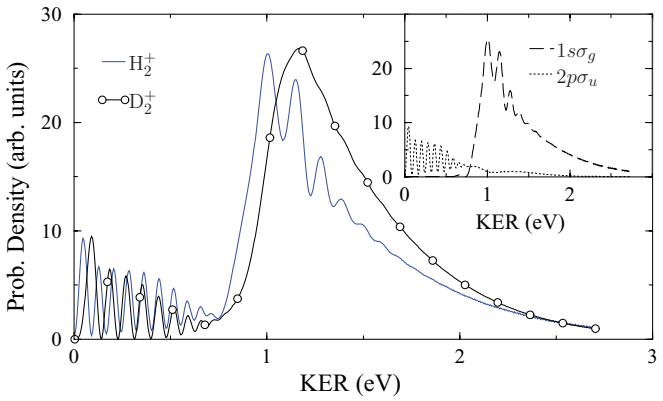

FIG. 3. (Color online) Model calculation of the KER for dissociation following ionization of a neutral target in a 790-nm 40-fs 10^{14}-W/cm^2 Gaussian laser pulse. The shift in peak position between the isotopes is clear. The inset shows the separate $1s\sigma_g$ and $2p\sigma_u$ contributions for H_2^+.

conclude that the intensity was at least 2×10^{13} W/cm^2 by comparison with the adiabatic Floquet potentials.

We can check the consistency of our arguments by solving the time-dependent Schrödinger equation (TDSE) for H_2^+ including only the $1s\sigma_g$ and $2p\sigma_u$ channels and assuming nonrotating aligned nuclei. Details of the calculation are given in Ref. [12]. The H_2 ground vibrational wave function was propagated on the $1s\sigma_g$ channel, starting at the time when the laser intensity was first high enough to ionize H_2, 8×10^{13} W/cm^2 in this case, but the results do not depend sensitively on this choice. The results are shown in Fig. 3. The inset shows that the majority of the wave packet dissociates to $1s\sigma_g$, which corresponds to 2ω ATD, or, in Floquet notation, the $1s\sigma_g - 2\omega$ ATD channel. The remainder dissociates via $2p\sigma_u$, or the $2p\sigma_u - 1\omega$ BS channel. The dominance of ATD over BS is consistent with our fit in Fig. 2. Moreover, the $1s\sigma_g - 2\omega$ distribution peaks at 1 eV, while $2p\sigma_u - 1\omega$ contributes at low KER. Both of these energies match the peak shifts in Fig. 2, and are consistent with our conclusion that the shifts are determined primarily by the initiating dissociation step.

Given the restrictions imposed by our model, both fits in Fig. 2 agree with the data well—except possibly for KER near 4 eV. The data are not sufficient to make any firm conclusion, but the possibility of a missed peak led us to check other sources of structure. We checked initiation by higher-order ATD and laser-induced electronic excitation, but the most plausible mechanism yielding an ~4-eV peak is ionization following electron-impact excitation by the rescattering electron. Assuming excitation upon its first return, a 4.0–4.6-eV KER peak (depending on the precise initial H_2^+ vibrational distribution) would indeed result from three-photon ionization of $2p\pi_u$. If we admit this possibility, however, then we have to allow the rest of the $2p\pi_u$ ATCE peaks. These peaks would overlap the spectrum in Fig. 2, contributing to the apparent broadening of the peaks. Their presence should be clear in a $\cos\theta$ KER spectrum, though, since the rescattering initiated ATCE peaks should appear relatively broad compared to the dissociation-initiated ATCE peaks—$\cos^8\theta$ rather than $\cos^{24}\theta$ [8].

C. D_2^+

It remains to explain the KER shift of the D_2^+ spectrum relative to the H_2^+ spectrum. Not surprisingly, we believe it derives from the mass difference. The potentials in Fig. 1 are the same in both cases, so the mean energy of the D_2^+ wave packets are also the same. Consequently, the wave packets' mean velocities are lower than for H_2^+. Only the higher velocity components of the wave packet reach a given crossing during the laser pulse. Thus, by keeping the pulse lengths the same for both species, a larger fraction of the low-energy components of the D_2^+ wave packet are cut off than for the corresponding H_2^+ wave packet, yielding KER peaks shifted to higher values. If this argument is correct, then it should hold also for peaks in the dissociation KER spectra, which can again be checked with the TDSE. The results are shown in Fig. 3, and the D_2^+ dissociation peak is indeed shifted to higher KER relative to H_2^+ for the same laser pulse. This velocity argument also explains the relative enhancement of the high-KER peaks in the D_2^+ spectra compared to H_2^+—the dissociating D_2^+ wave packet simply does not have enough time to reach the large-R (low-KER) crossings with as much amplitude as the H_2^+ wave packet.

IV. SUMMARY

While we have been able to glean considerable dynamical information from these spectra using our model, one can easily imagine that a pump-probe experiment would more directly reveal the time-dependent dynamics. The KER peaks corresponding to each of the ionization-threshold potential crossings should show strong enhancement when the pump-probe

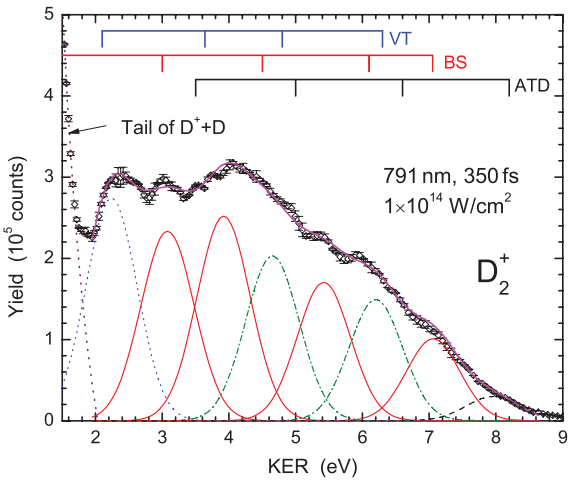

FIG. 4. (Color online) Experimental KER spectrum of D_2^+ ionization integrated over a 2° cone around the laser polarization from the two-dimensional spectrum in Fig. 4 of Ref. [13]. The vertical bars indicate the predicted KER peak locations, grouped by initiating mechanism as in Fig. 2. The low-KER tail, labeled in the figure, was fit (dotted purple line) and subtracted before fitting the Gaussians. This subtraction was necessary as only D^+ fragments were measured. The spectrum thus had contributions from both $D^+ + D^+$ and $D^+ + D$ channels, although primarily in different KER ranges [13]. Solid red lines indicate the individual BS peaks; dotted blue lines, VT peaks; dashed black lines, ATD peaks; and dot-dashed green lines, combined peaks. The solid purple line is the total fitted spectrum.

delay matches the corresponding travel times. Moreover, the cleanest version of this experiment would begin from an H_2^+ so that dissociation could be initiated with a pump pulse too weak to ionize. In any case, the probe pulse should have an intensity near the ionization appearance intensity and a length less than about 5 fs.

We have described the application of our model to the extensive near-appearance intensity data of Staudte *et al.*, emphasizing the insight it provides into the time-dependent dynamics of the system. Our model provides an explanation of the surprising structure, describing essentially all of the trends visible in the data including the intensity, polarization, and species dependence as well as the positions and relative widths of the peaks themselves. The data further support the ionization mechanism predicted by our model: ATCE. Our model, in turn, implies that a KER distribution in this intensity regime *cannot* simply be converted to an R distribution using $1/R$. Our model accomplishes all of these things without the need for any complicated calculation, only the plotting of the potential curves.

To close, we include one further brief illustration of the application of our model. This example is not for a neutral target as discussed previously, but rather for a D_2^+ beam target as in our original proposal for the ATCE mechanism [8]. The data, however, were taken by Pavičić *et al.* under long-pulse conditions [13], and were some of the first to show structure in the proton spectrum following ionization by an intense laser pulse. Since, at 350 fs, the pulse length was much longer than the Staudte *et al.* experiments, crossings with ionization channels at much larger values of R were accessible. This, in turn, resulted in ionization peaks at lower KER. Another consequence of this long pulse is the fact that some of the BS peaks have a significant downward shift in energy as only the lower vibrational levels undergo bond softening close enough in time to the intensities needed to ionize. Figure 4 shows the Pavičić *et al.* data and our model fit to it. Our model was applied in the same way discussed here and in Ref. [8].

ACKNOWLEDGMENTS

We acknowledge fruitful conversations with C. L. Cocke and are grateful to A. Staudte *et al.* and D. Pavičić *et al.* for sharing their data. Work supported by the Chemical Sciences, Geosciences, and Biosciences Division, Office of Basic Energy Sciences, Office of Science, US Department of Energy.

[1] A. S. Alnaser, X. M. Tong, T. Osipov, S. Voss, C. M. Maharjan, B. Shan, Z. Chang, and C. L. Cocke, Phys. Rev. A **70**, 023413 (2004).
[2] M. Thompson, M. Thomas, P. Taday, J. Posthumus, A. Langley, L. Frasinski, and K. Codling, J. Phys. B **30**, 5755 (1997).
[3] T. Zuo and A. D. Bandrauk, Phys. Rev. A **52**, R2511 (1995); T. Seideman, M. Y. Ivanov, and P. B. Corkum, Phys. Rev. Lett. **75**, 2819 (1995).
[4] I. Ben-Itzhak *et al.*, Phys. Rev. A **78**, 063419 (2008).
[5] Th. Ergler, A. Rudenko, B. Feuerstein, K. Zrost, C. D. Schröter, R. Moshammer, and J. Ullrich, Phys. Rev. Lett. **95**, 093001 (2005).
[6] J. H. Posthumus, Rep. Prog. Phys. **67**, 623 (2004).
[7] A. Staudte *et al.*, Phys. Rev. Lett. **98**, 073003 (2007).
[8] B. D. Esry, A. M. Sayler, P. Q. Wang, K. D. Carnes, and I. Ben-Itzhak, Phys. Rev. Lett. **97**, 013003 (2006).
[9] X. Urbain, B. Fabre, E. M. Staicu-Casagrande, N. de Ruette, V. M. Andrianarijaona, J. Jureta, and J. H. Posthumus, Phys. Rev. Lett. **92**, 163004 (2004).
[10] A. Giusti-Suzor, F. H. Mies, L. F. DiMauro, E. Charron, and B. Yang, J. Phys. B **28**, 309 (1995).
[11] D. Telnov and S. I. Chu, Phys. Rep. **390**, 1 (2004).
[12] P. Q. Wang, A. M. Sayler, K. D. Carnes, J. F. Xia, M. A. Smith, B. D. Esry, and I. Ben-Itzhak, Phys. Rev. A **74**, 043411 (2006).
[13] D. Pavičić, A. Kiess, T. W. Hänsch, and H. Figger, Phys. Rev. Lett. **94**, 163002 (2005); (private communication).